Coherence Quantum Beats in Two-Dimensional Electronic Spectroscopy

Yuan-Chung Cheng and Graham R. Fleming*

Department of Chemistry and QB3 Institute, University of California, Berkeley and Physical Bioscience Division, Lawrence Berkeley National Laboratory, Berkeley, California 94720

Received: November 12, 2007; In Final Form: February 13, 2008

We study the coherence quantum beats in two-dimensional (2D) electronic spectroscopy of a coupled dimer system using a theoretical method based on a time-nonlocal quantum master equation and a recently proposed scheme for the evaluation of the third-order photon echo polarization [Gelin, M. F.; Egorova, D.; Domcek, W. *J. Chem. Phys.* **2005**, *123*, 164112]. The simulations show that the amplitude and peak shape beating in the 2D spectra is a result of the interplay between the rephasing and non-rephasing contributions to the 2D signals and can be used to elucidate the coherence dynamics in a multichromophoric system. In addition, the results suggest that the rephasing and non-rephasing 2D spectra contain complementary information, and a study of both of them could provide more dynamical information from 2D electronic spectroscopy.

1. Introduction

The advent of two-dimensional (2D) electronic spectroscopy[1−3] has provided a direct probe of electronic couplings and excitation energy-transfer pathways in complex multilevel quantum systems. The 2D technique correlates the absorption and emission frequencies of the material system and thereby provides a map showing electronic couplings between electronic excitations and spectral diffusion between two transition energies. In particular, 2D cross peaks can elucidate electronic couplings and energy-transfer dynamics in complex multichromophoric systems,[4−6] while analysis of 2D line shape can reveal solvation dynamics and solute−solvent interactions in the condensed phase.[7−9] Applications to molecular *J* aggregates,[8] photosynthetic light-harvesting complexes,[10−12] and semiconductor quantum wells[13] have demonstrated that 2D electronic spectroscopy is a versatile and powerful probe for dynamical information.

A powerful aspect of 2D electronic spectroscopy is its capability to exploit the phase and coherence information in the time evolution of the optical polarization induced by the optical pulses. Pisliakov et al. first showed that these excitonic coherence effects will be manifested in quantum beats in 2D electronic spectra and can be related quantitatively to the coherence dynamics in the system.[5] Recently, quantum beats in 2D electronic spectra in the Fenna−Matthews−Olson bacteriochlorophyll (FMO) complex of green sulfur bacteria were observed, and the analysis of the beating patterns of diagonal peaks provided direct evidence of excitonic coherence in the system, that is, energy transfer in the FMO complex is described by wave-like motion rather than incoherent hopping.[12] However, while the beats in the cross peaks in 2D spectra are well characterized theoretically,[5,6,14,15] the origins of the amplitude and especially the peak shape beats in the diagonal peaks remain unclear. Since the cross peaks in 2D spectra are usually lower in amplitude and overlap with stronger diagonal peaks, an analysis based on the diagonal peaks is critical. Therefore, it is important that we understand the nature of the coherence beats in the diagonal peaks and formulate a prescription that can be applied to quantitatively extract coherence dynamical information from experimental 2D spectral data.

Recently, a method for the efficient calculation of third-order photon echo polarization was developed and applied to simulate a three-pulse photon echo peak shift and 2D electronic spectroscopy of a two-level electronic system coupled to explicit vibrational degrees of freedom.[16,17] This approach was later extended to treat two-exciton states for describing general third-order experiments on multichromophoric systems.[18] In an earlier work, we applied this density-matrix-based method to show that quantitative analysis of the time evolution of the cross peaks in 2D electronic spectroscopy can provide a complete understanding of the population and coherence dynamics for the system under study.[6] Because this approach is based on a time-nonlocal quantum master equation formalism that explicitly includes a field−matter interaction and non-Markovian effects,[19] all possible pulse-overlap effects and interferences between contributions from different Liouville pathways to the signal are included in the calculation. Therefore, this density-matrix-based method is ideal for investigating the electronic coherence effects and origin of quantum beats in the diagonal peaks in 2D electronic spectroscopy.

In this work, we apply the density matrix based method to study the 2D electronic spectroscopy of a model dimer system. Focusing on the time evolution of the amplitude and peak shape in 2D spectra, we aim to understand the origin of the amplitude and peak shape beating in 2D spectra and provide insights that can aid experimental studies. We also demonstrate that the rephasing and non-rephasing spectra of the model dimer system, when treated separately, can provide complementary dynamical information hidden in the total 2D spectra.

2. Theoretical Methods

2.1. 2D Electronic Spectroscopy. 2D electronic spectroscopy is a four-wave mixing experiment in which three laser fields interact with the sample to create a polarization and the signal in the phase-matching direction $\mathbf{k}_s = -\mathbf{k}_1 + \mathbf{k}_2 + \mathbf{k}_3$ is heterodyne-detected and Fourier-transformed with respect to the coherence time τ (the time delay between the first and second pulses) and the rephasing time t (the time delay between the

* To whom correspondence should be addressed. E-mail: GRFleming@lbl.gov.

10.1021/jp7107889 CCC: $40.75
Published on Web 04/01/2008

third pulse and the signal) to obtain the 2D electronic spectrum at a given population time T (the time delay between the second and third pulses).[1−3] Theoretically, the 2D electronic spectrum is described by the photon echo third-order polarization $P_{\mathrm{PE}}(t)$ in the phase-matching direction $\mathbf{k}_s = -\mathbf{k}_1 + \mathbf{k}_2 + \mathbf{k}_3$. We have demonstrated that by combining a time-nonlocal quantum master equation formalism[19,20] with a recently developed method for the calculation of third-order photon echo polarization,[16] the 2D electronic spectra for generalized multichromophoric systems can be calculated efficiently.[6] This approach is based on a reduced density matrix description of the system that incorporates all relevant optical fields into the Hamiltonian and propagates the driven dynamics of the system exactly, thereby including pulse-overlap effects and contributions from all Liouville pathways in the calculation. This enables proper simulation of 2D spectra at short population times. More importantly, all relevant dissipative dynamics of the system appear in the calculation. In the following, we briefly summarize this theoretical method for the calculation of 2D electronic spectra.

The time evolution of a quantum system driven by laser fields can generally be described by a quantum master equation ($\hbar = 1$)[21,22]

$$\dot{\rho}(t) = -i[H_{\mathrm{S}} + H_{\mathrm{int}}(t),\rho(t)] - \mathscr{R}[\rho(t)] \quad (1)$$

where $\rho(t)$ is the reduced density matrix of the electronic system, H_{S} is the electronic Hamiltonian, $H_{\mathrm{int}}(t)$ describes the interaction of the system with the laser fields, and $\mathscr{R}[\cdot]$ represents the dissipative dynamics of the system. We consider the dissipative dynamics induced by interactions of the system to a harmonic bath using the time-nonlocal (TNL) quantum master equation derived by Meier and Tannor.[19] This TNL formalism also treats the system−field interactions $H_{\mathrm{int}}(t)$ explicitly. In the electric point dipole approximation, $H_{\mathrm{int}}(t)$ can be written as

$$H_{\mathrm{int}}(t) = -\hat{\mu}\mathbf{E}(t) \quad (2)$$

where $\mathbf{E}(t)$ is the time-dependent electric field of the laser pulses and $\hat{\mu}$ is the electronic transition dipole operator defined by

$$\hat{\mu} = \sum_n \vec{\mu}_n(a_n + a_n^{\dagger}) \quad (3)$$

$$= X + X^{\dagger} \quad (4)$$

where a_n ($a_n^{\dagger}$) is the annihilation (creation) operator that destroys (creates) the nth excitation, and $\vec{\mu}_n$ is the transition dipole moment of the nth excitation. In the rotating-wave approximation (RWA), the three laser pulses in a photon echo experiment can be described by the time-dependent electric field

$$\mathbf{E}(t) = \sum_{a=1}^{3} [E_a(t - \tau_a)\exp\{-i(\bar{\omega}_a t - \mathbf{k}_a\cdot\mathbf{r})\} + \mathrm{c.c.}] \quad (5)$$

where τ_a represents the pulse central time, $E_a(t - \tau_a)$ is the laser pulse profile, $\bar{\omega}_a$ is the reduced carrier frequency of the field $\bar{\omega}_a = \omega_a - \omega_0$, and $\mathbf{k}_a$ is the momentum. In this work, we adopt a Gaussian pulse profile $E_a(t) \sim \exp(-4\ln 2(t - \tau_a)^2/\tau_p^2)$ and assume that all three pulses have a $\tau_p = 40$ fs duration and a carrier frequency $\omega_a = \omega_0$. Gelin et al. showed that within the RWA, $P_{\mathrm{PE}}(t)$ can be calculated by considering the time evolution of three auxiliary density matrices $\rho_1(t) - \rho_3(t)$ defined by the following dynamical equations[16,17]

$$\begin{aligned}
\partial_t\rho_1(t) &= -\mathrm{i}[\bar{H}_{\mathrm{S}} - V_1(t) - V_2^{\dagger}(t) - V_3^{\dagger}(t),\rho_1(t)] - \mathscr{R}[\rho_1(t)] \\
\partial_t\rho_2(t) &= -\mathrm{i}[\bar{H}_{\mathrm{S}} - V_1(t) - V_2^{\dagger}(t),\rho_2(t)] - \mathscr{R}[\rho_2(t)] \\
\partial_t\rho_3(t) &= -\mathrm{i}[\bar{H}_{\mathrm{S}} - V_1(t) - V_3^{\dagger}(t),\rho_3(t)] - \mathscr{R}[\rho_3(t)] \quad (6)
\end{aligned}$$

where

$$V_a(t) = E_a(t - \tau_a)\exp(\mathrm{i}\bar{\omega}_a t)X \quad (7)$$

Equation 6 is a system of three independent linear differential equations that can be efficiently solved by propagating the auxiliary density matrices numerically. The third-order photon echo polarization $P_{\mathrm{PE}}(t)$ can then be calculated using

$$P_{\mathrm{PE}}(t) = \langle X(\rho_1(t) - \rho_2(t) - \rho_3(t))\rangle \quad (8)$$

where the bracket $\langle ...\rangle$ means taking the expectation value of the operator and averaging over static disorder. $P_{\mathrm{PE}}(t)$ implicitly depends on the coherence time $\tau = \tau_2 - \tau_1$ and the population time $T = \tau_3 - \tau_2$ because $V_a(t)$ depends on the pulse central time τ_a. Note that to properly describe the third-order polarization, it is necessary to include contributions from the two-excitation states in eq 6. To this end, we expand all system operators in the ground and one-excitation subspace to the two-excitation manifold. This allows treatment of excitonic dynamics in the one- and two-excitation subspace in a consistent manner.[18]

With $P_{\mathrm{PE}}(t)$, the total 2D Fourier-transformed spectrum in the limit of ideal resolution is then given by double Fourier transform of the photon echo polarization field with respect to τ and t

$$S_{\mathrm{T}}(\omega_\tau,T,\omega_t) \sim \int_{-\infty}^{\infty}\mathrm{d}\tau\int_{-\infty}^{\infty}\mathrm{d}t\,\mathrm{e}^{-\mathrm{i}\omega_\tau\tau}\mathrm{e}^{\mathrm{i}\omega_t t}\times \mathrm{i}P_{\mathrm{PE}}(\tau,T,t) \quad (9)$$

where ω_τ is the coherence frequency and ω_t is the rephasing frequency. Note that while the 2D signal $S(\omega_\tau,T,\omega_t)$ is a complex function, we will consider exclusively the real value spectrum in this work.

We further divide the contributions from negative and positive τ pulse orderings and define the rephasing spectrum

$$S_{\mathrm{R}}(\omega_\tau,T,\omega_t) \sim \int_{0}^{\infty}\mathrm{d}\tau\int_{-\infty}^{\infty}\mathrm{d}t\,\mathrm{e}^{-\mathrm{i}\omega_\tau\tau}\mathrm{e}^{\mathrm{i}\omega_t t}\times \mathrm{i}P_{\mathrm{PE}}(\tau,T,t) \quad (10)$$

and the non-rephasing spectrum

$$S_{\mathrm{NR}}(\omega_\tau,T,\omega_t) \sim \int_{-\infty}^{0}\mathrm{d}\tau\int_{-\infty}^{\infty}\mathrm{d}t\,\mathrm{e}^{-\mathrm{i}\omega_\tau\tau}\mathrm{e}^{\mathrm{i}\omega_t t}\times \mathrm{i}P_{\mathrm{PE}}(\tau,T,t) \quad (11)$$

The rephasing spectrum has $\tau \geq 0$ pulse ordering and contains contributions from Liouville pathways that result in rephasing of induced dipoles in an inhomogeneous distribution of transition energies (photon echo signals). In contrast, the non-rephasing spectrum has $\tau \leq 0$ pulse ordering and contains contributions from free induction decay signals. The interplay between the S_{R} and S_{NR} contributions determines the 2D peak shape and can be used to characterize spectral diffusion in the system.[9,23,24] Previous studies of 2D electronic spectroscopy almost exclusively focused on the total spectrum because the total spectrum exhibits absorptive peak shape that avoids artificial phase twist and can be directly related to the linear absorption spectrum of the system. However, in this work, we will study all three variants of the 2D spectrum and demonstrate that additional spectral features related to dynamical information about the system can be obtained by study the rephasing and non-rephasing spectra separately.

2.2. Model Dimer System. To study the coherence quantum beats in 2D electronic spectroscopy, we consider a system with two electronically coupled chromophores described by the Frenkel-exciton Hamiltonian

$$H_S = \epsilon_g|0\rangle\langle 0| + \epsilon_1 a_1^\dagger a_1 + \epsilon_2 a_2^\dagger a_2 \quad (12)$$

$$+ J(a_1^\dagger a_2 + a_2^\dagger a_1) \quad (13)$$

where $|0\rangle$ denotes the electronic ground state, a_n ($a_n^\dagger$) is the annihilation (creation) operator that destroys (creates) an excitation at site $n = 1,2$, ϵ_g is the energy of the ground state, ϵ_1 and ϵ_2 are the site energies of an excitation localized at chromophores 1 and 2, respectively, and J is the electronic coupling between the two excitations.

The total system-plus-bath Hamiltonian is given by

$$H_T = H_S + H_{int}(t) + H_B + H_{SB} \quad (14)$$

where $H_{int}(t)$ is the system−field interactions defined in eqs 2 and 3, H_B is the Hamiltonian of a harmonic bath of independent harmonic oscillators, and H_{SB} describes the system−bath interactions. For the system−bath interactions, we assume that the electronic system is coupled linearly and diagonally to the bath through a number of collective bath coordinates

$$H_{SB} = -\sum_{n=1}^{2} a_n^\dagger a_n \cdot q_n \quad (15)$$

where q_n denotes a collective bath coordinate that is local to the nth chromophore in the system. Such excitation−bath couplings induce diagonal transition-energy fluctuations in the site representation. For simplicity, we assume that the bath coupled to each chromophore is described by the same Ohmic spectral function with an exponential cutoff

$$J(\omega) = \gamma_0 \omega \exp(-\omega/\omega_c)$$

where γ_0 is the coupling strength and ω_c is the cutoff frequency of the bath. We also assume that baths coupled to chromophores 1 and 2 are independent, that is, the cross-correlation function is $\langle q_1(t)q_2(0)\rangle = 0$.

In this work, we study a system with electronic coupling $J = 150\ \text{cm}^{-1}$ and with site energies of each chromophore relative to the renormalization frequency ω_0 given by $E_1 = -50\ \text{cm}^{-1}$ and $E_2 = 50\ \text{cm}^{-1}$. In the exciton representation, the two excitonic states e_1 and e_2 have relative energies of about $-158\ \text{cm}^{-1}$ and $158\ \text{cm}^{-1}$, respectively. Effectively, we choose to set the laser carrier frequency ω_0 to be centered between the two electronic transitions and apply the RWA so that all transition frequencies are reduced by ω_0. The bath parameters for the model system are $\gamma_0 = 1$ and $\omega_c = 150\ \text{cm}^{-1}$, and all of the simulations are carried out at 77 K. The bath reorganization energy

$$\lambda = \frac{1}{\pi}\int_0^\infty J(\omega)\mathrm{d}\omega$$

is $\sim 48\ \text{cm}^{-1}$, which is significantly smaller than the electronic coupling $J = 150\ \text{cm}^{-1}$. This corresponds to weak system−bath coupling so that the TNL quantum master equation based on the weak coupling approximation is applicable. Diagonal energetic static disorder characterized by a Gaussian distribution with $\sigma = 50\ \text{cm}^{-1}$ for both chromophores is included in the system. Furthermore, the transition dipole moments of the two localized transitions are assumed to have the same amplitudes and be orthogonal to each other. To account for the orientational factor, we consider an all-parallel setup for the three laser pulse polarizations and an isotropic distribution of fixed molecules.

To simulate the 2D electronic spectra for the model dimer system, we apply the TNL quantum master equation to propagate eqs 6 and 7 and calculate the photon echo polarization $P_{PE}(\tau,T,t)$ according to eq 8. For the 2D electronic spectrum at a given population time T, we compute $P_{PE}(\tau,T,t)$ on a two-dimensional grid of coherence time (τ) and rephasing time (t) points and then perform numerical fast Fourier transform on the 2D grid according to eqs 9−11 to obtain the total, rephasing, and non-rephasing 2D spectra, respectively. Monte Carlo sampling with 1000 random realizations of H_S and molecular orientations is used to average over the distribution of static disorder and transition dipole orientations.

3. Results and Discussion

In Figure 1, we show theoretical 2D spectra for the model dimer system at population times $T = 0$, 100, 150, and 200 fs. In addition to the real value total 2D spectra (eq 8), the rephasing (eq 9) and non-rephasing (eq 10) spectra are also shown. These 2D spectra exhibit two diagonal peaks (DP1 and DP2) corresponding to the two exciton states, respectively, and two cross peaks (CP12 and CP21) due to electronic coupling between them. At $T = 0$, the spectra already exhibit cross peaks between the two transitions, which represent contributions from excitonic coherence generated purely by the optical excitations. The rephasing and non-rephasing spectra show phase-twisted peak shapes, in which the rephasing peaks are elongated along the diagonal direction and the non-rephasing peaks are elongated along the antidiagonal direction.[23,25] In addition, the amplitudes of the rephasing peaks are significantly higher than those of the non-rephasing peaks. This contrast in rephasing and non-rephasing amplitudes is a manifestation of the inhomogeneity in the system. Because the inhomogeneous broadening in the rephasing spectra is partially eliminated by the photon echo effect, the rephasing pulse sequence gives rise to stronger signals than the free induction decay signals given by the non-rephasing pulse sequence.

Even for this simple dimer system, the 2D spectra in Figure 1 already display a wealth of information about the electronic population relaxation dynamics. For example, the two diagonal peaks in the total spectrum at $T = 0$ fs (correlation spectrum) exhibit significantly different peak shapes and amplitudes because of the population dynamics; the rounder and smaller DP2 diagonal peak shows additional dephasing of the coherence involving the upper exciton level (e_2) due to the $e_2 \rightarrow e_1$ energy transfer in the coherence time (τ) and rephasing time (t) periods (lifetime broadening). These dynamical 2D line shape effects are captured in our theoretical simulations because the density-matrix-based method for the evaluation of third-order photon echo polarization employed here describes the non-Markovian electronic relaxation dynamics of the dimer system at all time periods. Moreover, the population time evolution of the 2D spectra clearly shows the decay of the DP2 diagonal peak and the correlated emergence of a positive contribution to the CP21 cross peak on the time scale of $\sim$200 fs, which is indicative of the time scale of the $e_2 \rightarrow e_1$ energy transfer. The manifestation of population relaxation dynamics in the 2D spectroscopy has been extensively studied previously.[1,2,4,6,8,11,25] Therefore, in the following, we will focus on the beating in the 2D spectra and the coherence dynamics.

The total 2D spectrum in Figure 1 clearly shows beats in 2D diagonal and cross peaks as a function of T. In particular, the

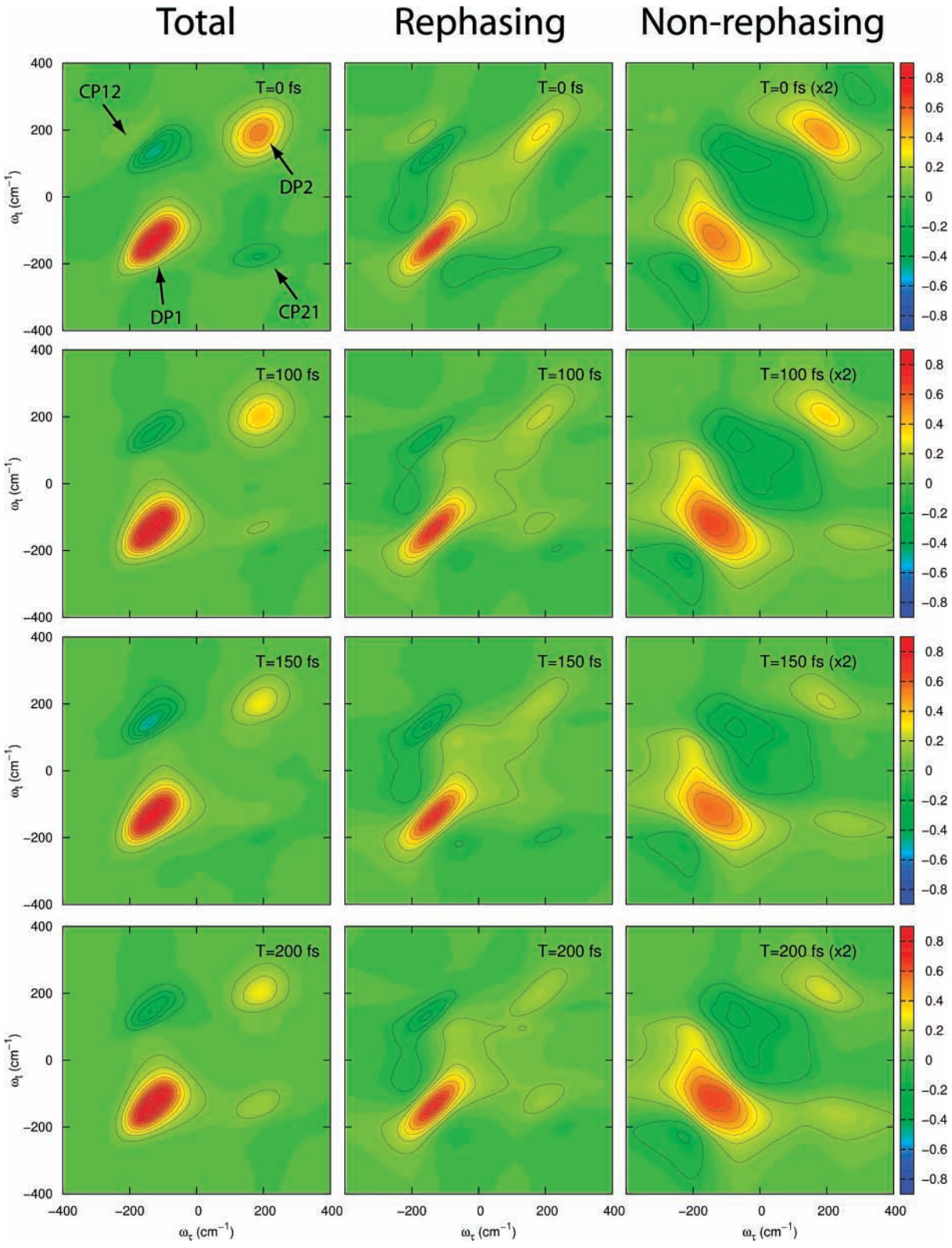

Figure 1. Theoretical real value 2D spectra for the model dimer system at population times $T = 0$, 100, 150, and 200 fs. At each T, the real value total spectrum (left), the real value rephasing spectrum (center), and the real value non-rephasing spectrum (right) are shown. The x and y axes are, respectively, the coherence frequency and the rephasing frequency relative to the carrier frequency of the laser ω_0. Two diagonal peaks (DP1 and DP2) and two cross peaks (CP12 and CP21) can be clearly seen at all T. The maxima of the lower and upper diagonal peaks on the total spectrum are at approximately -130 and 200 cm^{-1}, respectively. The absorption maxima are blue shifted from the relative transition energies of the two exciton states (at -158 and 158 cm^{-1}, respectively) because of the system−bath interactions (i.e., Stokes shift). The negative features are in blue, and positive features are in yellow and red. The upper cross peaks, CP12, is mostly negative because it is dominated by the excited-state absorption contributions that are negative in the real value 2D spectrum. Note that all of the total and rephasing spectra are shown on the same scale, while the non-rephasing spectra are scaled by 2.

DP1 diagonal peak shows correlated beats in its amplitude and peak shape; when the amplitude is stronger ($T = 100$ and 200 fs), the peak is rounder, and when the amplitude is weaker ($T = 0$ and 150 fs), the peak is more elongated. This is precisely

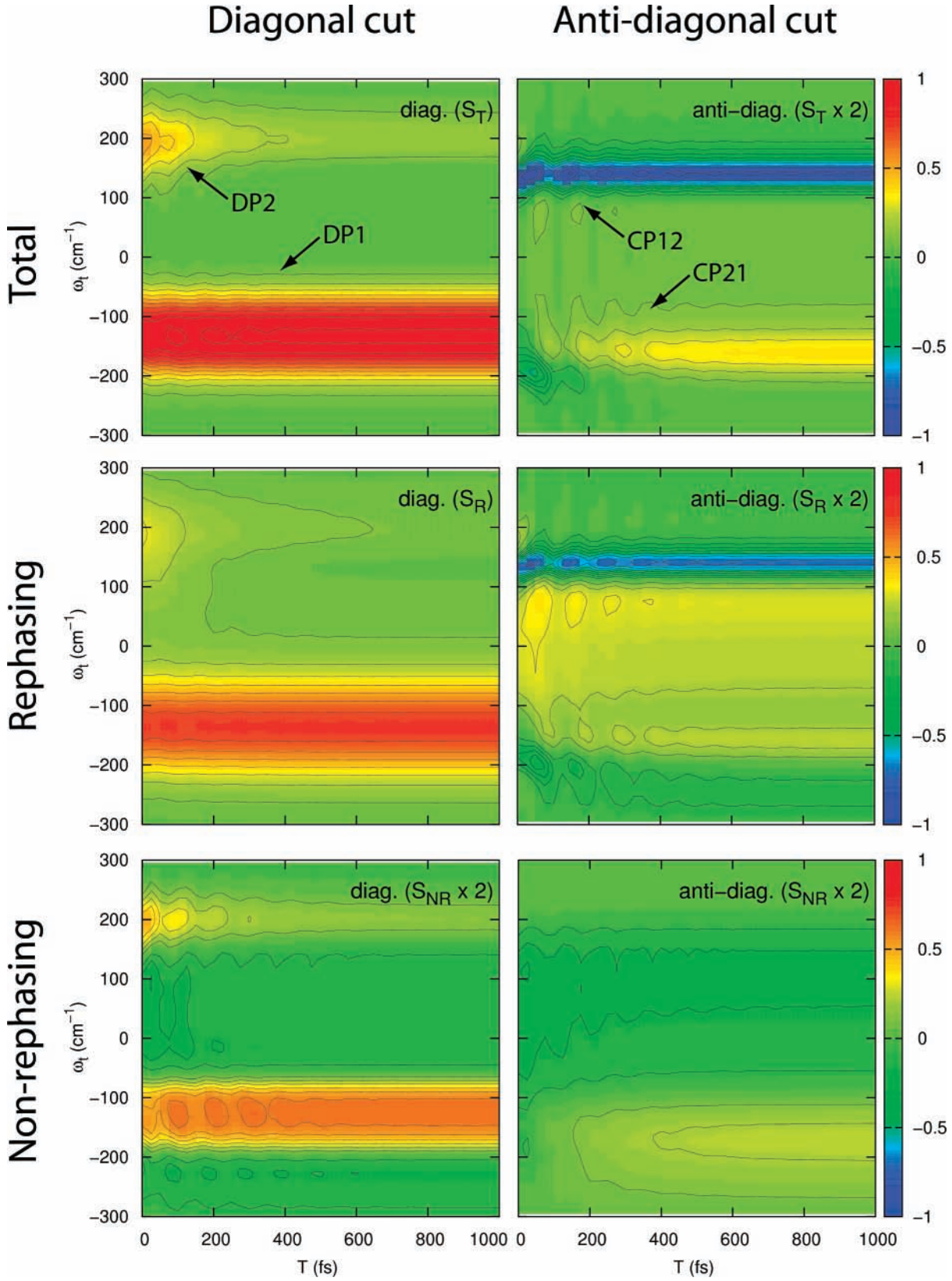

Figure 2. Time evolution of the diagonal cut through the diagonal peaks (left panel) and the antidiagonal cut through the off-diagonal peaks (right panel) of the 2D spectra. Clearly, the beating in the diagonal peaks is dominated by the non-rephasing contributions to the 2D signals. In contrast, the beating in the cross peaks is dominated by the rephasing contributions. Note that the weak beating in the antidiagonal cut of the non-rephasing spectrum is due to interference from the diagonal peaks.

what has been observed in the experimental 2D spectra in the FMO complex.[12] A closer inspection reveals that this peak shape beating is due to coherence beats in the amplitude of the non-rephasing contribution to the total 2D spectrum. Because the non-rephasing peak shape is elongated along the antidiagonal direction, a stronger non-rephasing contribution results in a rounder peak in the total 2D spectrum. Therefore, the peak shape beating in the 2D spectra is a result of the interplay between

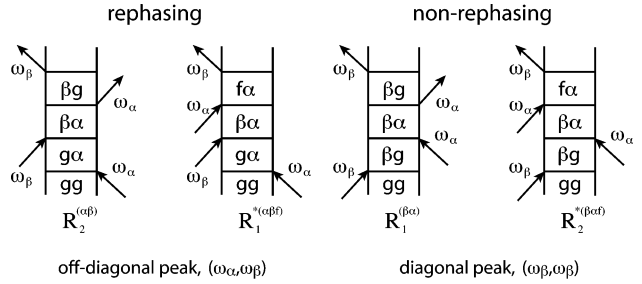

Figure 3. The impulsive limit double-sided Feynman diagrams representing contributions to the third-order polarization from the coherence pathways. In these diagrams, g denotes the ground state, the Greek letters denote one-exciton states, and f represents a two-exciton state. For these pathways, the system is prepared in a coherence state $|\alpha\rangle\langle\beta|$ during the population time T; therefore, an oscillating phase factor with a frequency of $\Delta E_{\alpha\beta}$ is associated with all of these terms. Note that because the $\tau > 0$ (rephasing) and $\tau < 0$ (non-rephasing) contributions have different orderings of the first two pulses, the rephasing contributions give rise to cross peaks on a 2D spectrum, while the non-rephasing contributions give rise to diagonal peaks.

the rephasing and non-rephasing contributions to the 2D signals. In addition, Figure 1 shows that while the amplitude of the rephasing contribution to the DP1 diagonal peak remains constant in T, the non-rephasing contribution exhibits quantum beats. In contrast, the cross peaks (e.g., the CP12 cross peak) show pronounced beats in the rephasing spectra but remain constant in the non-rephasing spectra.

To follow the time evolution of the 2D spectra more closely, we take a diagonal cut (through the diagonal peaks) and an antidiagonal cut (through the two cross peaks) for each 2D spectrum and plot the cuts as a function of T (Figure 2). The time evolution of these cuts shown in Figure 2 provides a clear visualization of the population and coherence dynamics in the system. In addition, the beats in the diagonal peaks are clearly dominated by the non-rephasing contributions to the 2D signals, and, in contrast, the beats in the cross peaks are dominated by the rephasing contributions. This contrast can be explained by considering the coherence Liouville pathways that give rise to the 2D signals in the impulsive limit.[14,27,28] In Figure 3, we show the double-sided Feynman diagrams representing these coherence pathways, in which the system is in a coherence state $|\beta\rangle\langle\alpha|$ ($\alpha \neq \beta$) during the population time T. Because the time evolution of the coherence state has an oscillating phase factor with the frequency equal to the energy difference between the pair of exciton states ($\Delta E_{\alpha\beta} = E_\beta - E_\alpha$), these contributions cause excitonic quantum beats in the 2D spectra. Importantly, when divided into the rephasing and the non-rephasing contributions, coherence pathways contribute to the cross peaks in rephasing spectra; however, in non-rephasing spectra, the coherence pathways contribute to the diagonal peaks. Note that our simulation is not based on the response function formalism and is thus not limited to the contributions from these Liouville pathways alone. Nevertheless, the Feynman diagrams in Figure 3 provide a convenient and intuitive explanation of the amplitude and peak shape beating in 2D spectroscopy.

Since the coherence pathways that give rise to excitonic quantum beats in 2D spectra contribute differently in the rephasing and non-rephasing pulse sequences, we suggest that by looking at the cross peaks in the 2D rephasing spectrum and the diagonal peaks in the 2D non-rephasing spectrum, one can further deconvolute the contributions due to excitonic coherence from those due to energy-transfer dynamics and extract the coherence dynamics more clearly. In Figure 4a, we plot the amplitude of the DP1 diagonal peak in the non-

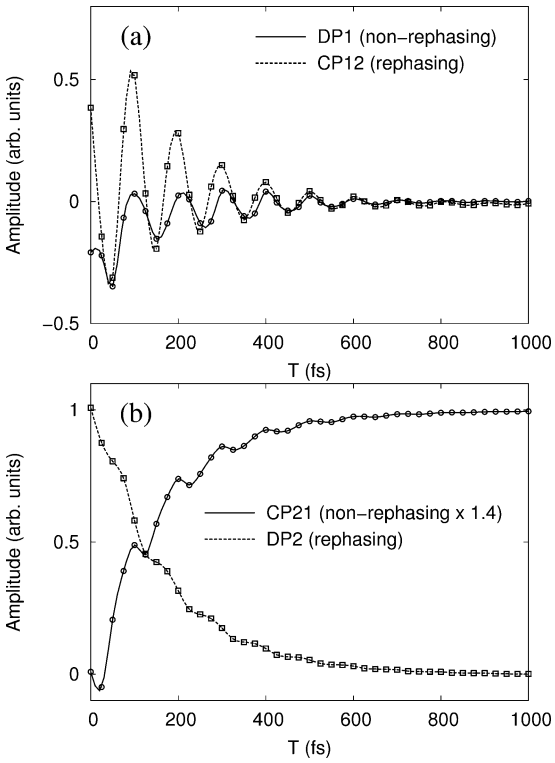

Figure 4. Amplitude of 2D peaks as a function of population time. (a) A comparison between the amplitude beating of the DP1 diagonal peak in the non-rephasing spectra (solid line) and that of the CP12 cross peaks in the rephasing spectra (dashed line). The beating period of ∼105 fs corresponds to the energy gap of ∼316 cm^{-1} between the two exciton states. In addition, the dephasing time of ∼400 fs can be extracted from the damping of the beats. For clear comparison, the two curves are shifted so that their long time value approaches zero. (b) We plot the peak amplitude evolution of the CP21 cross peaks in the non-rephasing spectra (solid line) and the DP2 diagonal peak in the rephasing spectra (dashed line). The $e_2 \rightarrow e_1$ energy transfer on the time scale of ∼200 fs can be clearly seen. For clear comparison, the two curves are shifted so that their minima values approach zero, and the curve for the CP21 non-rephasing peak is scaled so that its value approaches 1 at long population time. Note that the weak beats in both the CP21 and DP2 curves are due to interference from the diagonal peaks and off-diagonal peaks, respectively.

rephasing spectra (solid line) and the CP12 cross peaks in the rephasing spectra (dashed line). Quantum beats at these two positions are correlated, as indicated by the Feynman diagrams in Figure 3. The period of ∼105 fs corresponds to an energy gap of ∼316 cm^{-1} between the two exciton states. In addition, the damping of the beats indicates that the dephasing time of the $|e_1\rangle\langle e_2|$ coherence is ∼400 fs. Note that for a multilevel quantum system, such coherence beats would have frequencies corresponding to energy gaps between exciton levels; therefore, spectral analysis of the beating frequencies can lead to relative eigen energies of the excitons. Furthermore, the quantum beats also provide information on the dephasing and coherence transfer dynamics in the system.[6,12] While the rephasing and non-rephasing spectra contain unwanted distortions of the 2D peak shape, investigating them separately provide a means to selectively study contributions from different Liouville pathways by different pulse orderings.[29]

Evidently, the separation of rephasing and non-rephasing spectra can also be useful for the extraction of population dynamics. In Figure 4b, we plot the peak amplitude evolution of the CP21 cross peaks in the non-rephasing spectra (solid line) and that of the DP2 diagonal peak in the rephasing spectra (dashed line). Figure 4b clearly shows the $e_2 \rightarrow e_1$ energy

transfer on the time scale of ~200 fs. The population dynamics is easily seen in the emergence of the positive contribution to the CP21 cross peaks in the non-rephasing spectrum and the decay of the DP2 diagonal peak in the rephasing spectrum (Figure 4b). Note that the sum of the values of the two curves in Figure 4b is approximately constant at all population times, indicating that the two curves directly correspond to the decay of the e_2 population and the increase of the e_1 population and all contributions not due to $e_2 \rightarrow e_1$ energy transfer are eliminated by examining the rephasing and non-rephasing contributions separately. Because the oscillatory coherence pathways do not contribute to the cross peaks in the non-rephasing spectrum and the diagonal peaks in the rephasing spectrum, separating the rephasing and non-rephasing contributions in 2D spectroscopy can avoid oscillatory features that could obscure the energy-transfer dynamics.

4. Conclusions

In this paper, a time-nonlocal quantum master equation coupled with a recently proposed scheme[16] for the evaluation of the third-order polarization in the phase-matching direction $\mathbf{k}_s = -\mathbf{k}_1 + \mathbf{k}_2 + \mathbf{k}_3$ was used to simulate the 2D electronic spectrum of a coupled dimer system. We demonstrated that the interplay of electronic coherence pathways in the rephasing and non-rephasing contributions to the total 2D spectrum results in the amplitude and peak shape beats in the diagonal peaks, and these quantum beats can be quantitatively related to the coherence dynamics in the system. The results provide a simple and intuitive explanation for the amplitude and peak shape beats recently observed in the 2D experiment on the photosynthetic FMO complex.[12] Moreover, we showed that the separation of rephasing spectra and non-rephasing spectra provides a means to further deconvolute contributions from different coherence pathways, making it valuable to investigate the two contributions separately. Although our model simulation is based on a simple dimer model, the results should be applicable to more general multilevel systems.

Previously, Khalil et al. have demonstrated for 2D infrared (IR) spectroscopy that amplitude beats due to coherence between states appear in diagonal peaks in non-rephasing spectra and in cross peaks in rephasing spectra.[26] Although they studied vibrational states, the same observations and conclusions are also applicable to electronic 2D spectroscopy considered in the present work. However, the effects of inhomogeneous broadening (peak shape beating) and of ultrafast relaxation dynamics were not discussed by Khalil et al. in ref 26. Our simulations included inhomogeneous effects, pulse-overlap effects, and full electronic relaxation dynamics in the dimer system and consequently demonstrated the peak shape beats and that the quantum beats in 2D electronic spectrum can be observed even when fast relaxation dynamics is present (Figure 2). More importantly, we have explicitly shown that coherence dynamics and relaxation dynamics can be studied independently by examining the rephasing and non-rephasing spectra separately. Therefore, the present theoretical study not only complements previous experimental observations in 2D IR[26] and electronic[12] spectroscopy but also presents new means to obtain dynamical information from experimental data.

The ellipticity of 2D diagonal peaks[30] and the relative amplitudes of the rephasing and non-rephasing contributions[9] have been suggested as measures of the frequency−frequency correlation function of the electronic system. Our results indicate that excitonic coherence effects can alter the peak shape of 2D peaks; therefore, the adaptation of these measures of correlation functions has to be treated carefully. In principle, the beating contribution due to excitonic coherence can be eliminated by fitting to a damped oscillatory function, and the remaining component would represent contributions from system−bath interactions.

Acknowledgment. This work was supported by the Office of Basic Energy Sciences, Chemical Sciences Division, U.S. Department of Energy (Contract DE-AC03-76SF000098). This research used resources of the National Energy Research Scientific Computing Center, which is supported by the Office of Science of the U.S. Department of Energy under Contract No. DE-AC02-05CH11231. Y.-C.C. thanks Gregory S. Engel and Elizabeth L. Read for helpful discussions.

References and Notes

(1) Mukamel, S. *Annu. Rev. Phys. Chem.* **2000**, *51*, 691.
(2) Jonas, D. M. *Annu. Rev. Phys. Chem.* **2003**, *54*, 425.
(3) Brixner, T.; Mancal, T.; Stiopkin, I. V.; Fleming, G. R. *J. Chem. Phys.* **2004**, *121*, 4221.
(4) Cho, M.; Vaswani, H. M.; Brixner, T.; Stenger, J.; Fleming, G. R. *J. Phys. Chem. B* **2005**, *109*, 10542.
(5) Pisliakov, A. V.; Mancal, T.; Fleming, G. R. *J. Chem. Phys.* **2006**, *124*, 234505.
(6) Cheng, Y.-C.; Engel, G. S.; Fleming, G. R. *Chem. Phys.* **2007**, *341*, 285.
(7) Hybl, J.; Yu, A.; Farrow, D.; Jonas, D. M. *J. Phys. Chem. A* **2002**, *106*, 7651.
(8) Stiopkin, I. V.; Brixner, T.; Yang, M.; Fleming, G. R. *J. Phys. Chem. B* **2006**, *110*, 20032.
(9) Roberts, S. T.; Loparo, J. J.; Tokmakoff, A. *J. Chem. Phys.* **2006**, *125*, 084502.
(10) Brixner, T.; Stenger, J.; Vaswani, H. M.; Cho, M.; Blankenship, R. E.; Fleming, G. R. *Nature* **2005**, *434*, 625.
(11) Zigmantas, D.; Read, E. L.; Mancal, T.; Brixner, T.; Gardiner, A. T.; Cogdell, R. J.; Fleming, G. R. *Proc. Natl. Acad. Sci. U.S.A.* **2006**, *103*, 12672.
(12) Engel, G. S.; Calhoun, T. R.; Read, E. L.; Ahn, T.-K.; Mancal, T.; Cheng, Y.-C.; Blankenship, R. E.; Fleming, G. R. *Nature* **2007**, *446*, 782.
(13) Li, X.; Zhang, T.; Borca, C.; Cundiff, S. *Phys. Rev. Lett.* **2006**, *96*, 057406.
(14) Cho, M.; Fleming, G. R. *J. Chem. Phys.* **2005**, *123*, 114506.
(15) Egorova, D. *Chem. Phys.* **2008**, doi:10.1016/j.chemphys.2007.12.019.
(16) Gelin, M. F.; Egorova, D.; Domcke, W. *J. Chem. Phys.* **2005**, *123*, 164112.
(17) Egorova, D.; Gelin, M. F.; Domcke, W. *J. Chem. Phys.* **2007**, *126*, 074314.
(18) Cheng, Y.-C.; Lee, H.; Fleming, G. R. *J. Phys. Chem. A* **2007**, *111*, 9499.
(19) Meier, C.; Tannor, D. J. *J. Chem. Phys.* **1999**, *111*, 3365.
(20) Kleinekathöfer, U. *J. Chem. Phys.* **2004**, *121*, 2505.
(21) Redfield, A. G. *IBM J. Res. Dev.* **1957**, *1*, 19.
(22) Breuer, H.-P.; Petruccione, F. *The Theory of Open Quantum Systems*; Oxford University Press: Oxford, U.K., 2002.
(23) Hybl, J.; Christophe, Y.; Jonas, D. M. *Chem. Phys.* **2001**, *266*, 295.
(24) Khalil, M.; Demirdoven, N.; Tokmakoff, A. *Phys. Rev. Lett.* **2003**, *90*, 047401.
(25) Tokmakoff, A. *J. Phys. Chem. A* **2000**, *104*, 4247.
(26) Khalil, M.; Demirdoven, N.; Tokmakoff, A. *J. Chem. Phys.* **2004**, *121*, 362.
(27) Mukamel, S. *Principles of Nonlinear Optical Spectroscopy*; Oxford University Press: Oxford, U.K., 1995.
(28) Zhang, W.; Chernyak, V.; Mukamel, S. *J. Chem. Phys.* **1999**, *110*, 5011.
(29) Ge, N. H.; Zanni, M. T.; Hochstrasser, R. M. *J. Phys. Chem. A* **2002**, *106*, 962.
(30) Lazonder, K.; Pshenichnikov, M. S.; Wiersma, D. A. *Opt. Lett.* **2006**, *31*, 3354.